Supplementary Information

for

A pyridine-woven covalent organic framework facilitating the immobilization of Co single atoms towards efficient photocatalytic H_2 evolution

Yanchi Yao,[a] Jingbo Lin,[a] Shasha Liu,[a] Yong Zheng,[b] Lun Lu,[c] Qile Fang,[d] Shuang Song,[a] Chao Zhu,*[a] Yi Shen*[a,e]

a Key Laboratory of Microbial Technology for Industrial Pollution Control of Zhejiang Province, College of Environment, Zhejiang University of Technology, Hangzhou, 310032, China.

b College of Materials and Chemical Engineering, China Three Gorges University, Yichang, 443002, China.

c State Environmental Protection Key Laboratory of Environmental Pollution Health Risk Assessment, Ministry of Ecology and Environment, South China Institute of Environmental Sciences, Guangzhou 510655, China.

d Advanced Institute of Natural Sciences, Beijing Normal University at Zhuhai, Zhuhai, 519087, China.

e Shaoxing Research Institute, Zhejiang University of Technology, Shaoxing, 312000, China.

*Corresponding Author Dr. Chao Zhu, Dr. Yi Shen. Email: zhuchao@zjut.edu.cn, shenyi@zjut.edu.cn; Fax: +86-571-88320276; Tel: +86-571-88320726.

Experimental Procedures

Materials

1,4-dicyanobenzene ($C_8H_4N_2$, 98%) and 2,6-pyridinedicarbonitrile ($C_7H_3N_3$, 97%) were purchased from Bide Pharmatech Co., Ltd. Trifluoromethanesulfonic acid (CF_3SO_3H, 99%), ethanol (C_2H_6O, AR), and cobaltous acetate tetrahydrate ($C_4H_6CoO_4{\cdot}4H_2O$, 99.9%) were purchased from Sinopharm Chemical Reagent Co., Ltd. Triethanolamine (TEOA, AR) was purchased from Shanghai Titan Scientific Co., Ltd. All the chemicals could be directly used without further purification.

Characterization

The functional groups and crystal structures of the samples were characterized using Fourier-transform infrared spectroscopy (FTIR) and X-ray diffraction (XRD). Scanning electron microscopy (SEM) and transmission electron microscopy (TEM) are employed to examine the morphology and internal structures. The dispersion of Co atoms was detected by Aberration-corrected high-angle annular dark-field scanning transmission electron microscopy (AC-HAADF-STEM) using a Titan 80-300 scanning/transmission electron microscope operated at 300 kV, equipped with a probe spherical aberration corrector. The element distribution was characterized by energy-dispersive X-ray spectroscopy (EDS) mapping. The chemical states and variations were investigated by X-ray photoelectron spectroscopy (XPS) on a Thermo Scientific ESCA-Lab200i-XL spectrometer (Waltham, MA) using monochromatic Al Alα radiation (1486.6 eV). UV-vis DRS studies were performed on a Shimadzu UV-2550 UV-vis spectrophotometer in the wavelength range of 200-800 nm using $BaSO_4$ as a reference for baseline. Photoelectrochemical tests, including electrochemical impedance spectroscopy (EIS), periodic on/off photocurrent responses, and Mott-Schottky plots, are conducted to determine the photoelectrochemical and electrochemical properties of the photocatalysts.

Photoelectrochemical measurements

The photoelectrochemical measurements were performed on a CHI 660E electrochemical workstation equipped with the three-electrode cell. Firstly, the original FTO glasses were cleaned with acetone, ethanol, and ultra-pure water. A fluorine-doped tin oxide (FTO) glass plate, a standard Ag/AgCl electrode, and a Pt electrode (20×20×0.1 mm) were employed as the working electrode, reference electrode, and counter electrode, respectively. A 300 W Xe lamp (PLS-SXE 300D/300DUV, Beijing Perfectlight) with a 400 nm cutoff filter was used as the light source. The transient photocurrent curves were measured at the open circuit potential with a 50-second light on/off cycle, and the 0.1 M Na_2SO_4 aqueous solution was used as the electrolyte. Mott-Schottky curves were tested at a frequency of 1 kHz and the applied voltage range of –0.5~1 V in a 0.001 M Na_2SO_4 solution. Electrochemical impedance spectroscopy (EIS) was obtained by applying an AC voltage of 5 mV amplitude in the frequency range from 10^6 to 0.1 Hz.

The working electrode of the glass FTO electrode was coated with the catalyst. FTO glass plates (2 × 2 cm) were used to attach the samples and its specific preparation method was as follows: First, the glass plates were ultrasonically cleaned sequentially with tap water, acetone, ethanol, and deionized water for 30 min respectively. Then, 20 mg of powder sample powder, 300 μL of isopropanol, and 300 μL of 20% Nafion solution were mixed by ultrasonic dispersion. Next, the 30 ul

dispersion was dropped into a 1 cm^2 square center area of the working area of the glass plates. At last, the sample was evenly dried under the natural wind.

The electrode potential (vs. Ag/AgCl) was converted to E_{RHE} by the following Eq.1 and 2.

$$E_{RHE\ pH=6.7} = E_{Ag/AgCl\ pH=6.7} + 0.059pH + 0.19 \quad (1)$$

$$E_{NHE\ pH=0} = E_{RHE\ pH=6.7} - 0.059pH \quad (2)$$

Band gap calculation

The band gap was estimated by following Tauc's relation equation:

$$(\alpha h\nu)^2 = \alpha_0(h\nu - E_g) \quad (3)$$

where h is Plank constant, ν is frequency of incident light, α_0 is absorption coefficient, E_g is optical band-gap and n is a constant.

Determination of apparent quantum yield (AQY)

The apparent quantum efficiency can be evaluated from following equation:

$$AQY = \frac{2 \times n_{H_2} \times N_A}{N} \quad (4)$$

Where n_{H_2} is the number of evolved H_2 molecules, N_A is the Avogadro number (6.02×10^{23}) and N represents the number of incident photons, which can be calculated from equation:

$$N = \frac{light\ intensity\ (W\ cm^{-2}) \times illumination\ area\ (cm^2)}{\frac{hc}{\lambda}} \quad (5)$$

where h is plank constant (6.626×10^{-34} J·s = 4.136×10^{-15} eV·s), c is the speed of light (3.0×10^8 m·s^{-1}), and λ is the wavelength of light. The irradiated area is 10 cm^2

The irradiated area, resulting n_{H_2}, and calculated AQY values are listed in Table S1.

XAFS data processing

The acquired EXAFS data were processed according to the standard procedures using the Athena and Artemis implemented in the IFEFFIT software packages. The fitting detail is described below:

The acquired EXAFS data were processed according to the standard procedures using the ATHENA module implemented in the IFEFFIT software packages. The EXAFS spectra were obtained by subtracting the post-edge background from the overall absorption and then normalizing with respect to the edge-jump step. Subsequently, the χ(k) data of were Fourier transformed to real (R) space using a hanning windows (dk=1.0 $Å^{-1}$) to separate the EXAFS contributions from different coordination shells. To obtain the quantitative structural parameters around central atoms, least-squares curve parameter fitting was performed using the ARTEMIS module of IFEFFIT software packages.[2]

The following EXAFS equation was used:

$$\chi(k) = \sum_j \frac{N_j S_0^2 F_j(k)}{kR_j^2} exp[-2k^2\sigma_j^2] exp[\frac{-2R_j}{\lambda(k)}] sin[2kR_j + \phi_j(k)] \quad (3)$$

S_0^2 is the amplitude reduction factor, $F_j(k)$ is the effective curved-wave backscattering amplitude, N_j is the number of neighbors in the j^{th} atomic shell, R_j is the distance between the Xray absorbing central atom and the atoms in the j^{th} atomic shell (backscatter), λ is the mean free path in Å, $\phi_j(k)$ is the phase shift (including the phase shift for each shell and the total central atom phase shift), σ_j is the Debye-Waller parameter of the j^{th} atomic shell (variation of distances around the average R_j). The functions $F_j(k)$, λ, and $\phi_j(k)$ were calculated with the ab initio code FEFF8.2. The additional details for EXAFS simulations are given below. The coordination numbers of model samples were fixed as the nominal values. The obtained S_0^2 was fixed in the subsequent fitting. While the internal atomic distances R, Debye-Waller factor σ^2, and the edge-energy shift ΔE_0 were allowed to run freely.

DFT calculations

All the DFT calculations were conducted based on the Vienna Ab-inito Simulation Package (VASP). The exchange-correlation effects were described by the Perdew-Burke-Ernzerhof (PBE) functional within the generalized gradient approximation (GGA) method. The core-valence interactions were accounted by the projected augmented wave (PAW) method. The energy cutoff for plane wave expansions was set to 400 eV, and the 3×3×1 Monkhorst-Pack grid k-points were selected to sample the Brillouin zone integration. The structural optimization was completed for energy and force convergence set at 1.0×10^{-4} eV and 0.05 eV $Å^{-1}$, respectively.

The Gibbs free energy change (ΔG) of each step is calculated using the following formula:

$$\Delta G = \Delta E + \Delta ZPE - T\Delta S \quad (6)$$

where ΔE is the electronic energy difference directly obtained from DFT calculations, ΔZPE is the zero point energy difference, T is the room temperature (298.15 K) and ΔS is the entropy change. ZPE could be obtained after frequency calculation by:

$$ZPE = \frac{1}{2}\sum hvi \quad (7)$$

And the TS values of adsorbed species are calculated according to the vibrational frequencies:

$$TS = k_B T \left[\sum_k ln(\frac{1}{1-e^{-hv/k_B T}}) + \sum_k \frac{hv}{k_B T} \frac{1}{(e^{hv/k_B T}-1)} + 1 \right] \quad (8)$$

Supplementary Figures

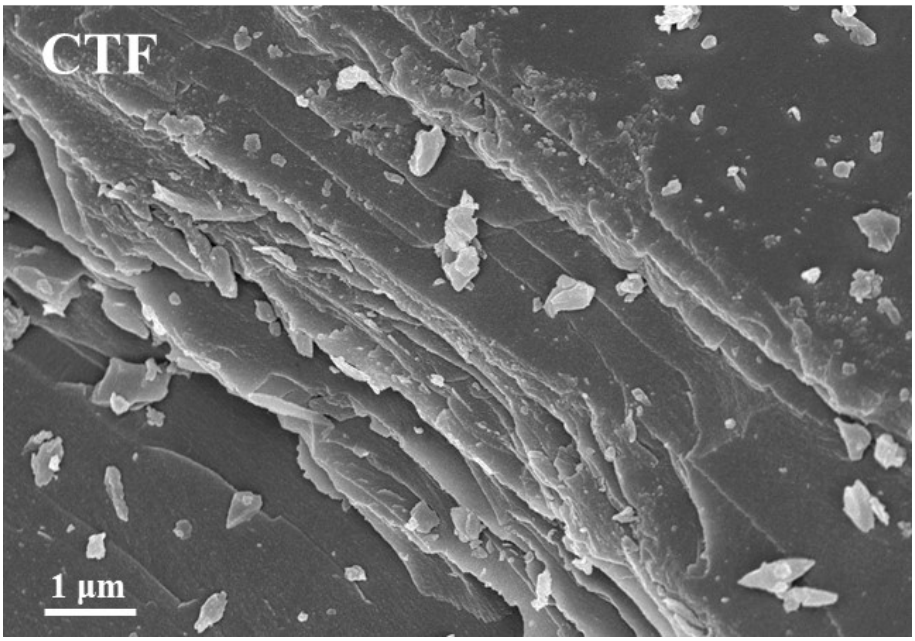

Fig. S1. SEM images of CTF.

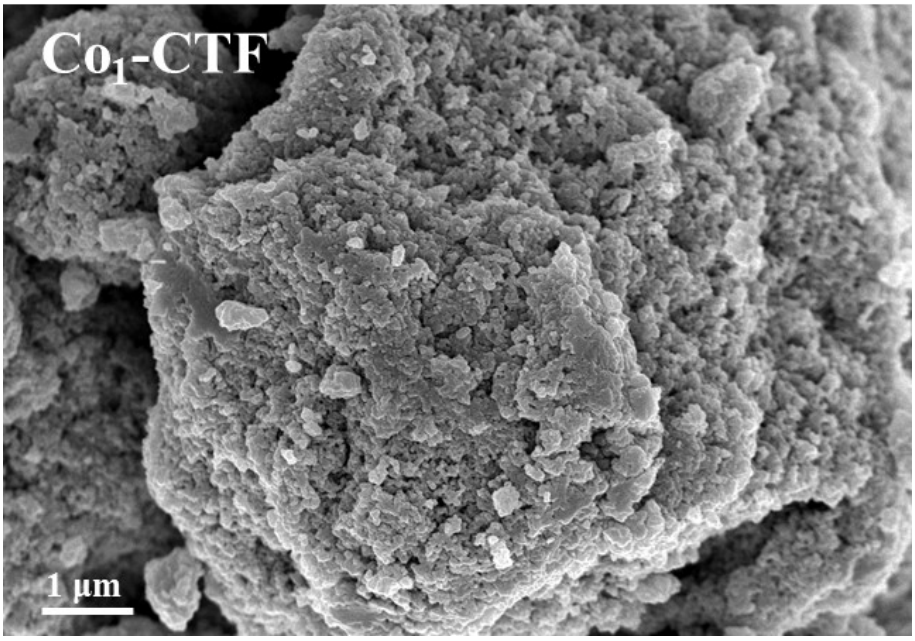

Fig. S2. SEM images of Co_1-CTF.

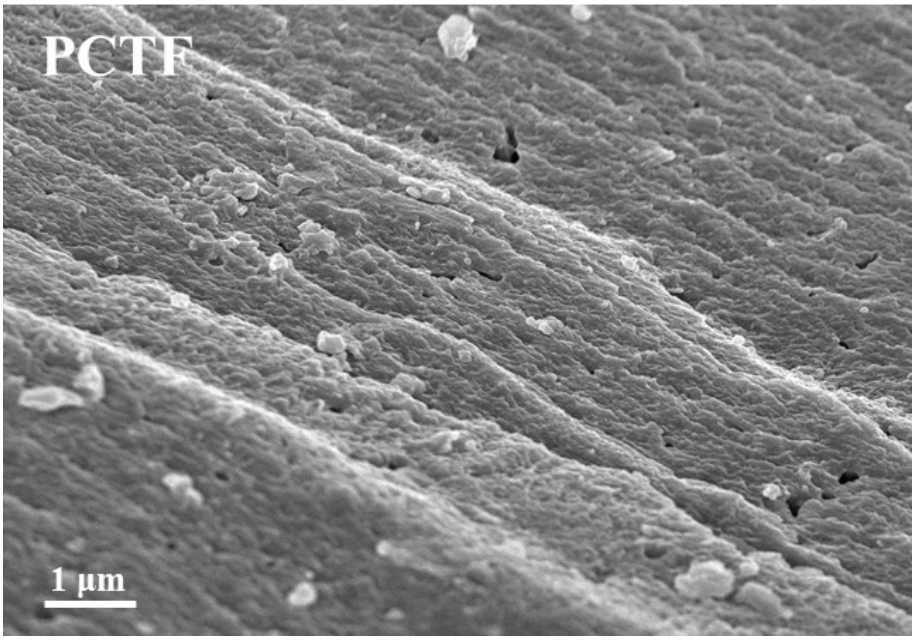

Fig. S3. SEM images of PCTF.

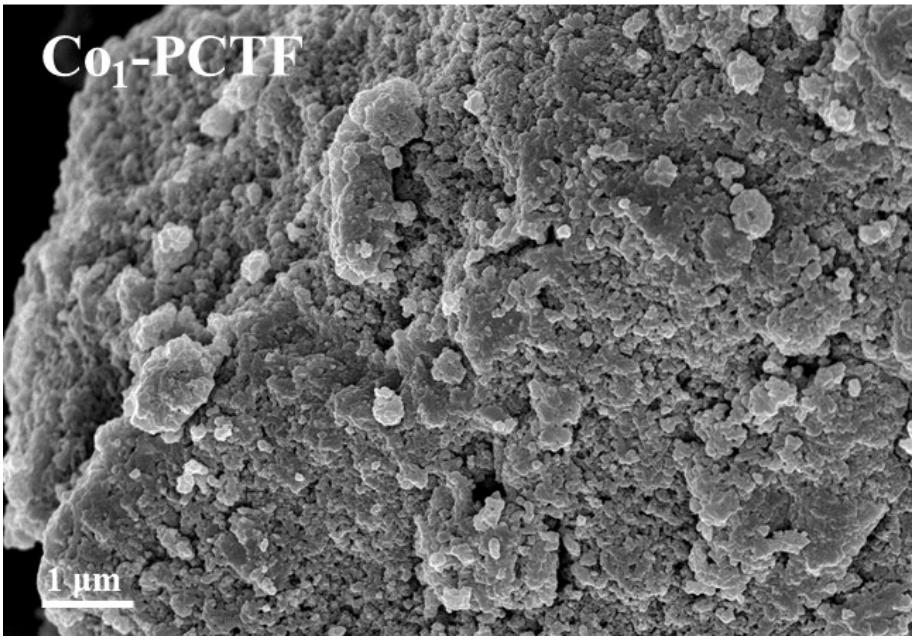

Fig. S4. SEM images of Co_1-PCTF.

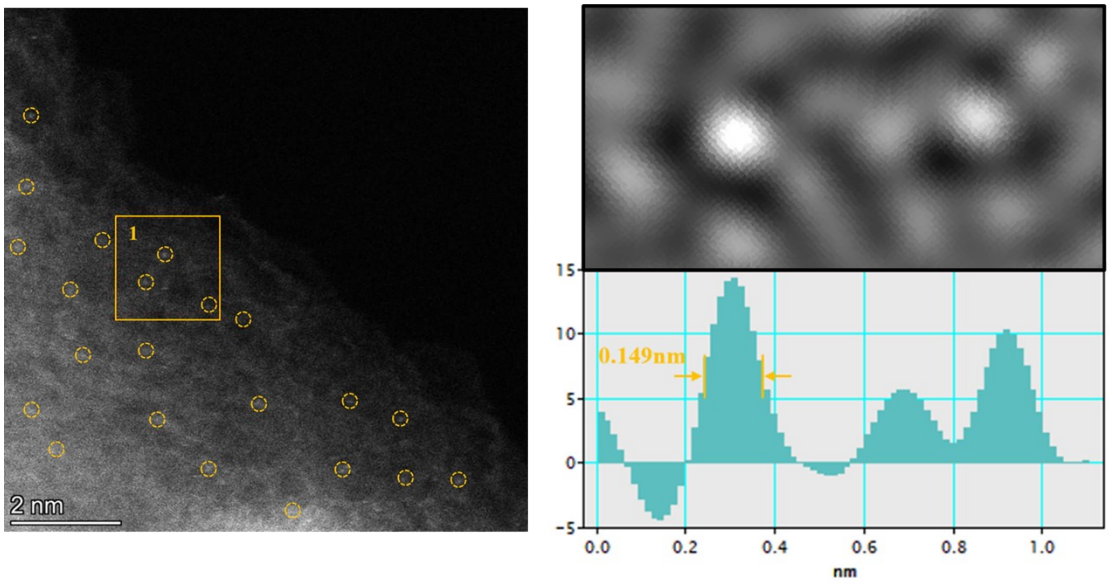

Fig. S5. Intensity profiles from the site 1.

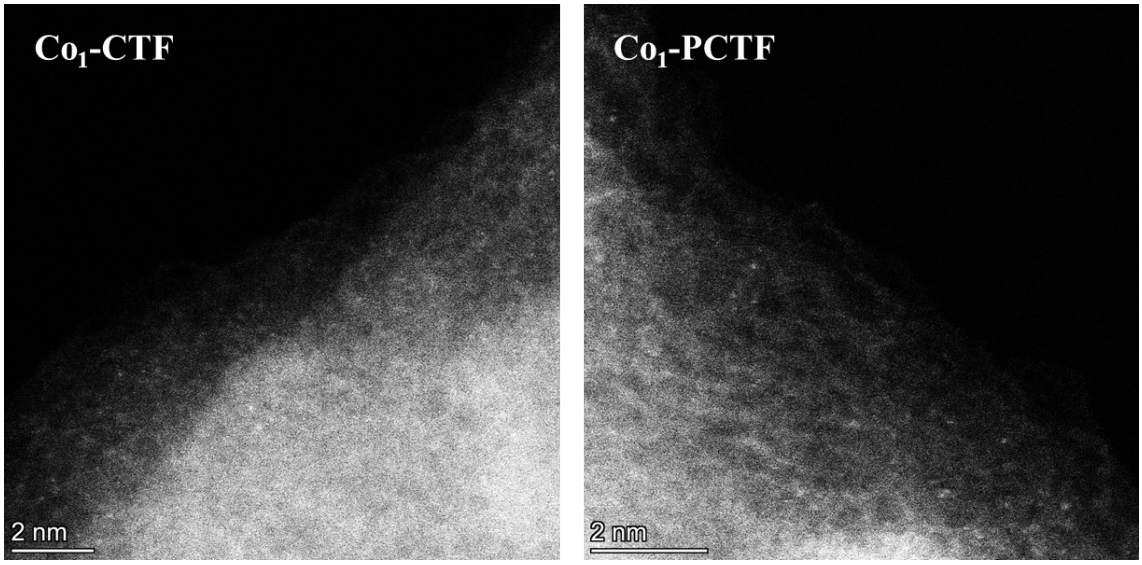

Fig. S6. HAADF-STEM image of (a) Co_1-CTF and (b) Co_1-PCTF.

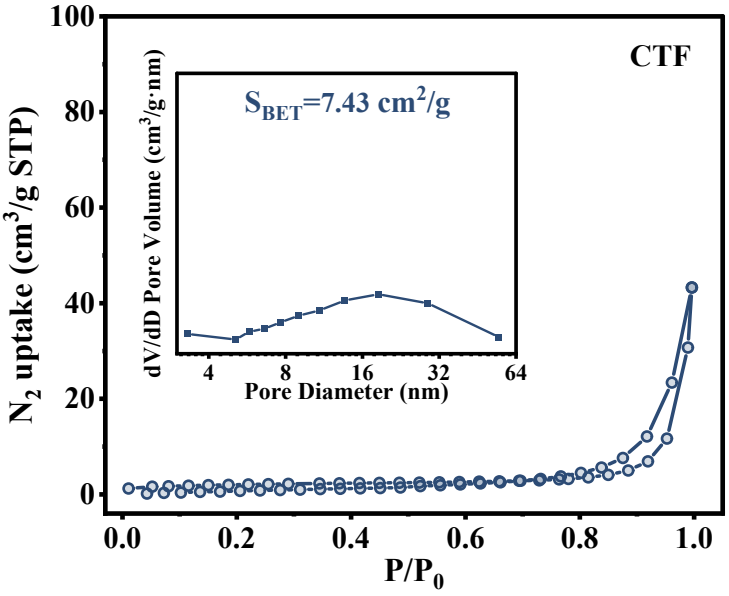

Fig. S7. N_2 adsorption and desorption isotherm and pore size distribution (inset) of CTF at 77 K.

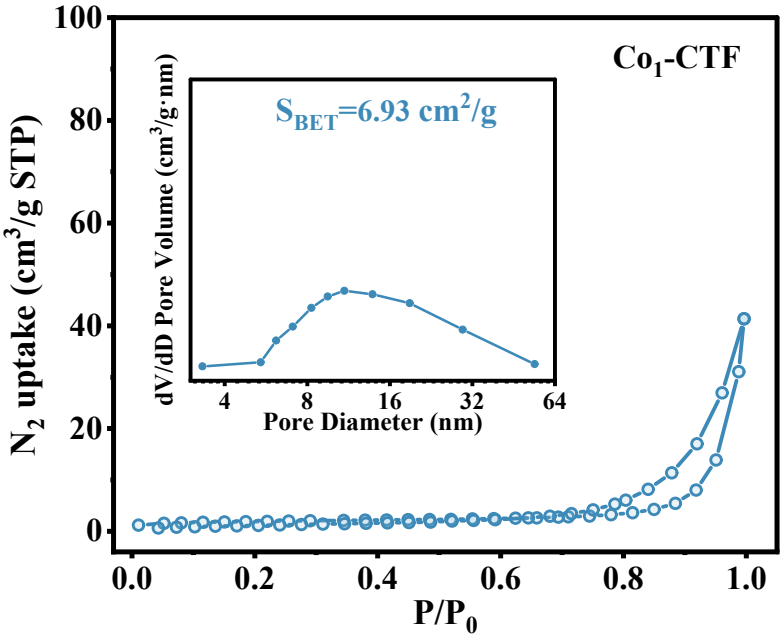

Fig. S8. N_2 adsorption and desorption isotherm and pore size distribution (inset) of Co_1-CTF at 77 K.

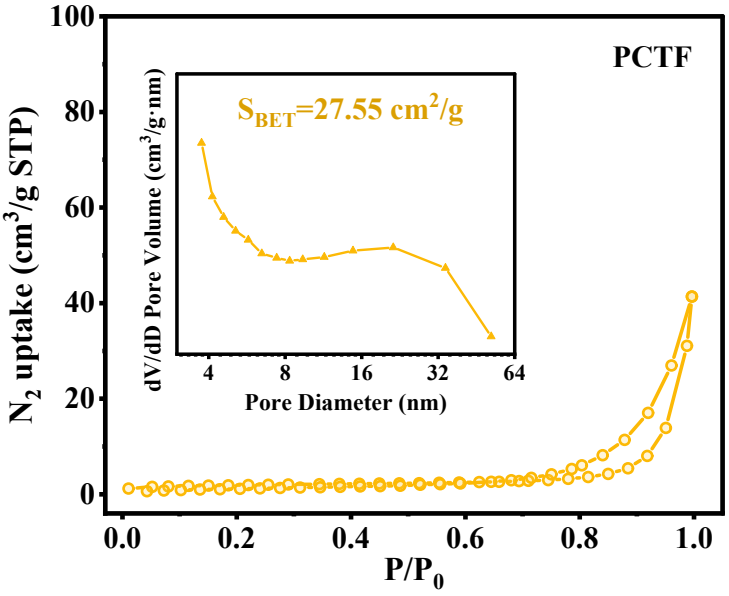

Fig. S9. N_2 adsorption and desorption isotherm and pore size distribution (inset) of PCTF at 77 K.

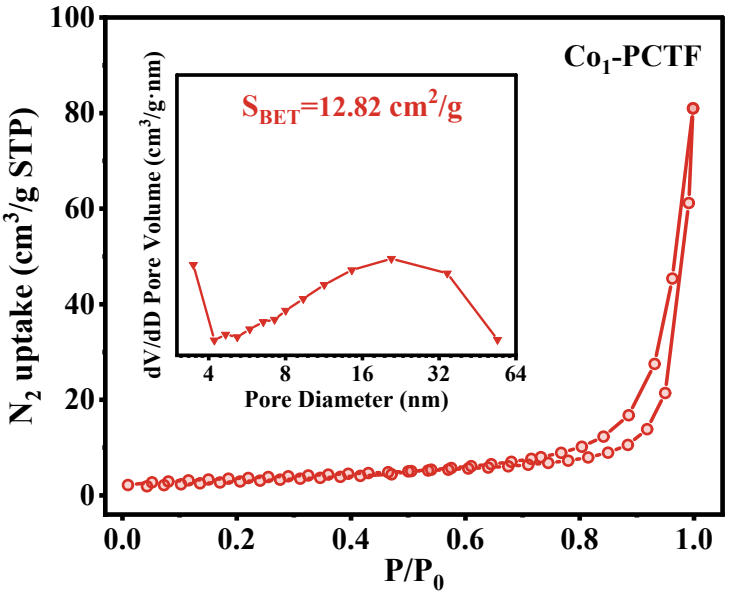

Fig. S10. N_2 adsorption and desorption isotherm and pore size distribution (inset) of Co_1-PCTF at 77 K.

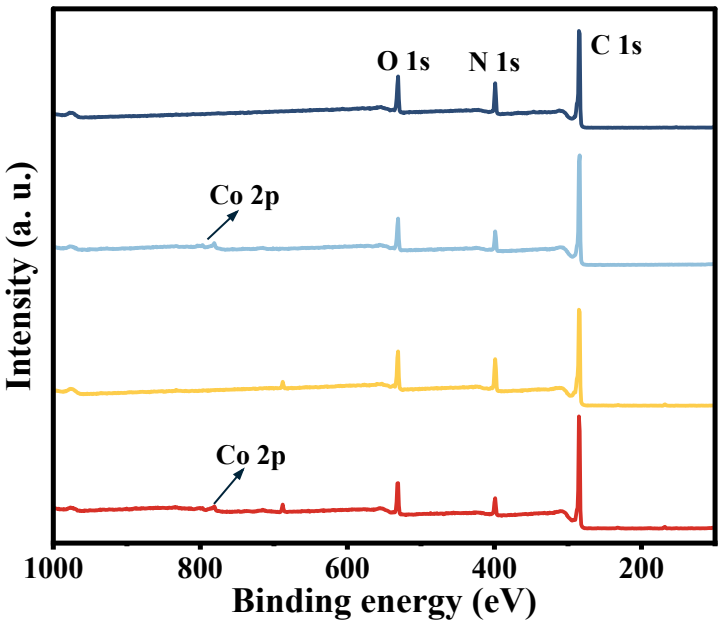

Fig. S11. XPS full spectra.

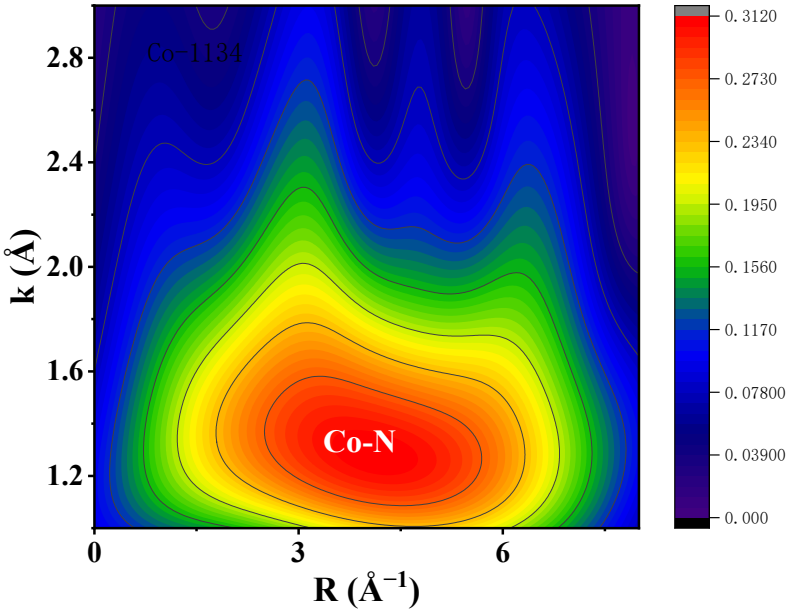

Fig. S12. The wavelet transform plot of Co_1-PCTF.

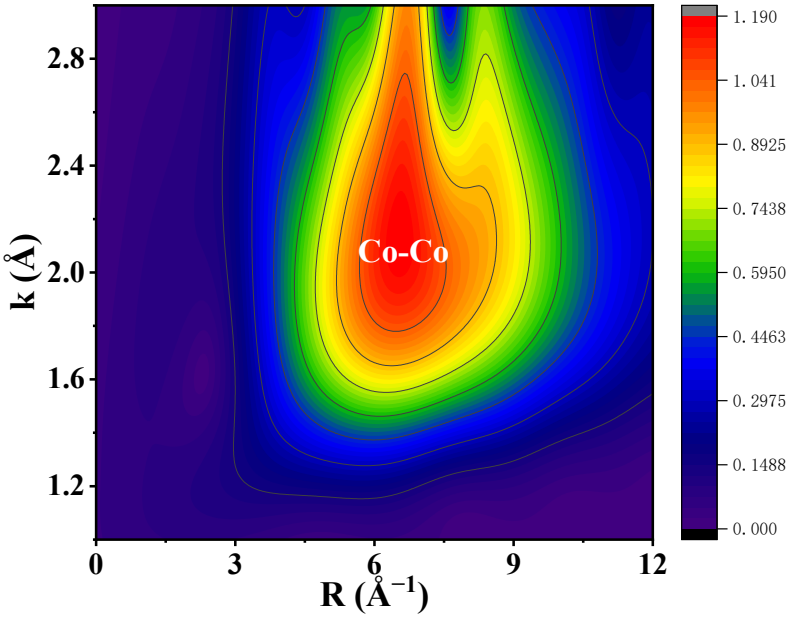

Fig. S13. The wavelet transform plot of Co foil.

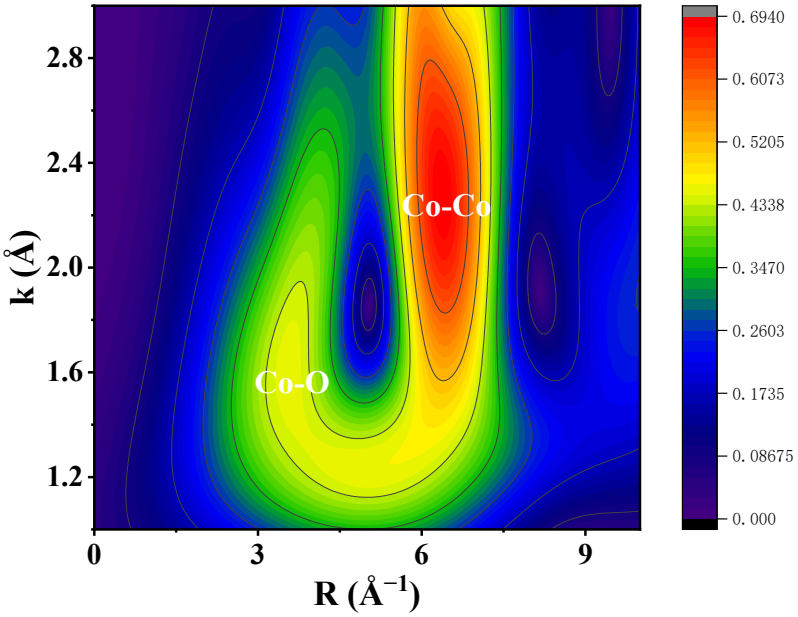

Fig. S14. The wavelet transform plot of Co_3O_4.

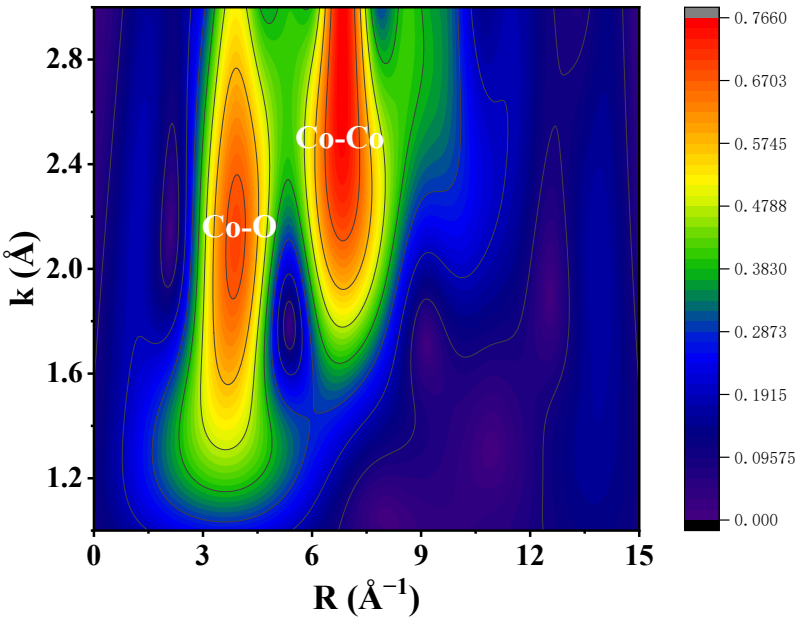

Fig. S15. The wavelet transform plot of CoO.

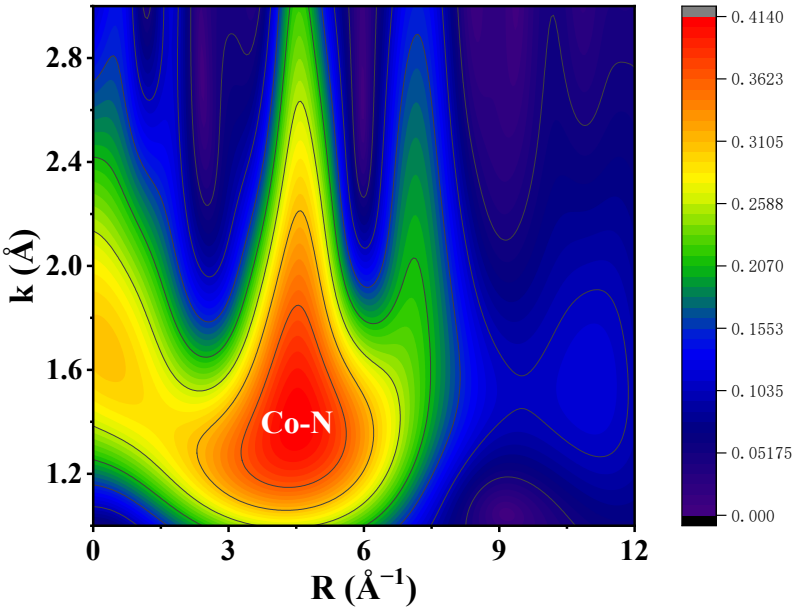

Fig. S16. The wavelet transform plot of CoPc.

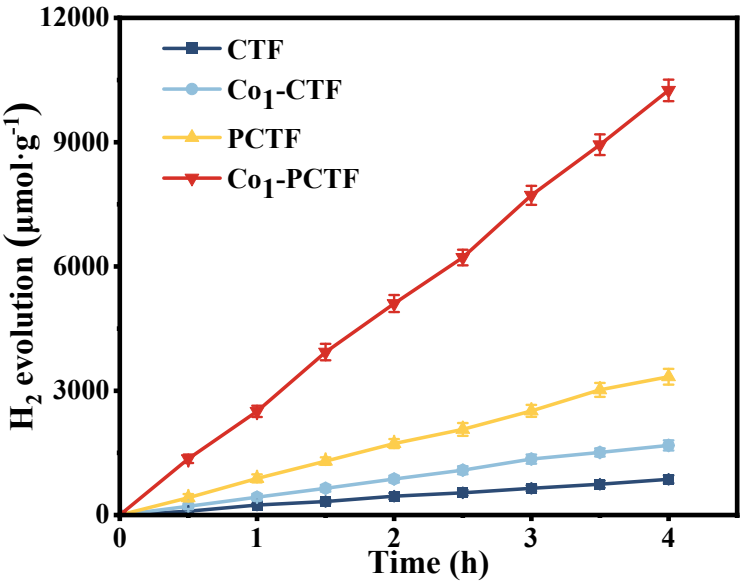

Fig. S17. Time-dependent course of photocatalytic H_2 evolution of as-prepared samples under 420 nm irradiation.

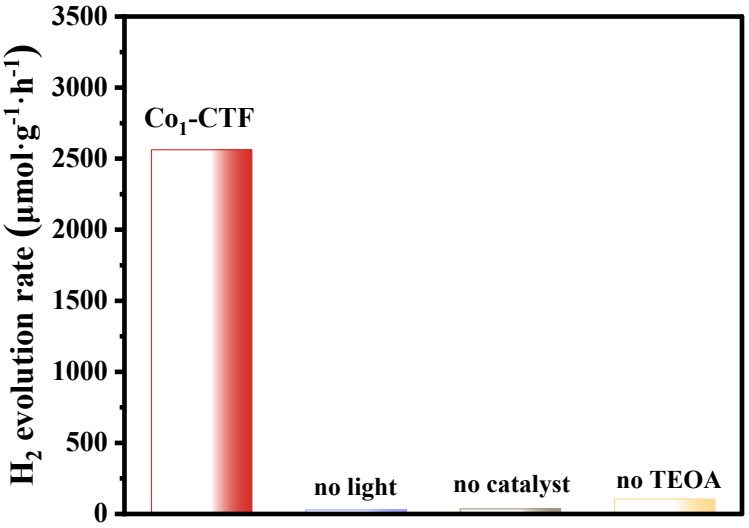

Fig. S18. The control experiments under the various conditions (without light, without catalyst, and without TEOA).

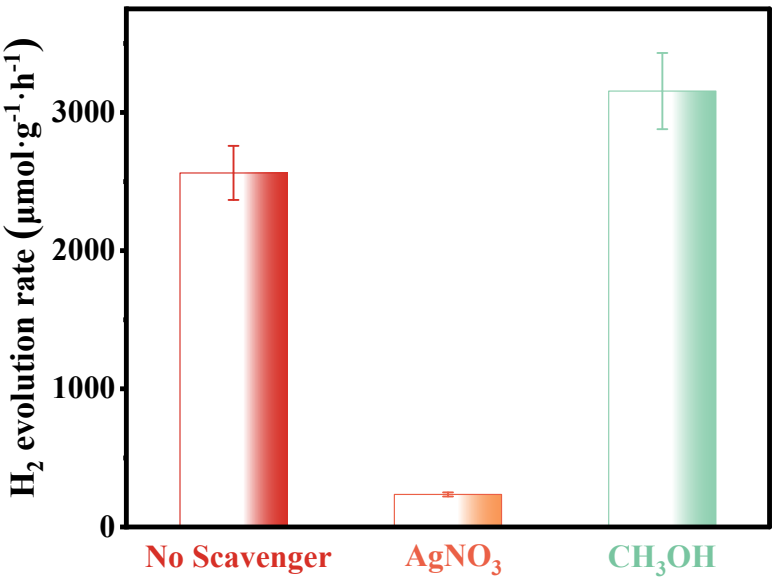

Fig. S19. The photocatalytic H_2 evolution rate when $AgNO_3$ or CH_3OH was added.

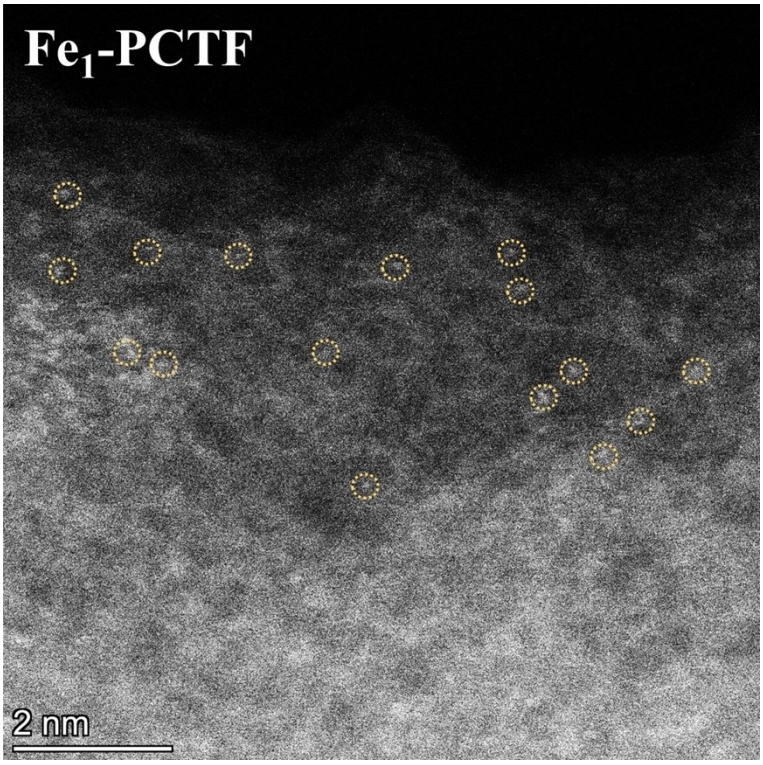

Fig. S20. The HAADF-STEM image of Fe_1-PCTF

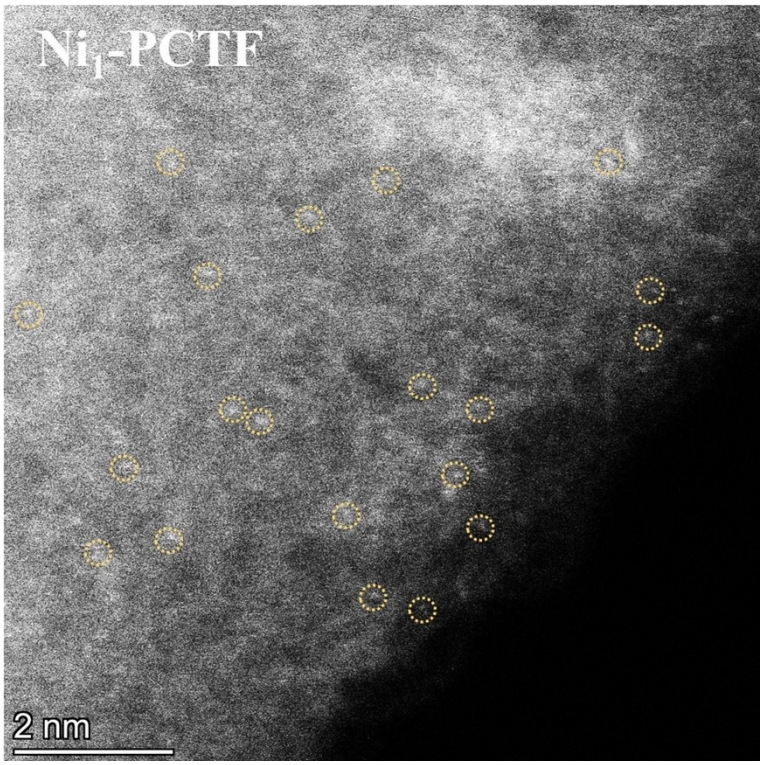

Fig. S21. The HAADF-STEM image of Ni_1-PCTF

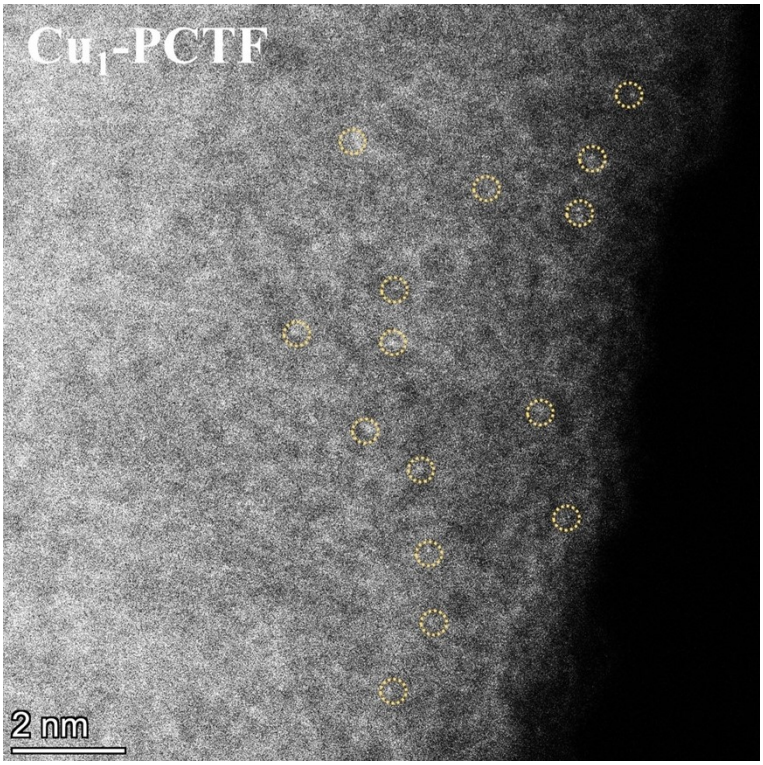

Fig. S22. The HAADF-STEM image of Cu_1-PCTF

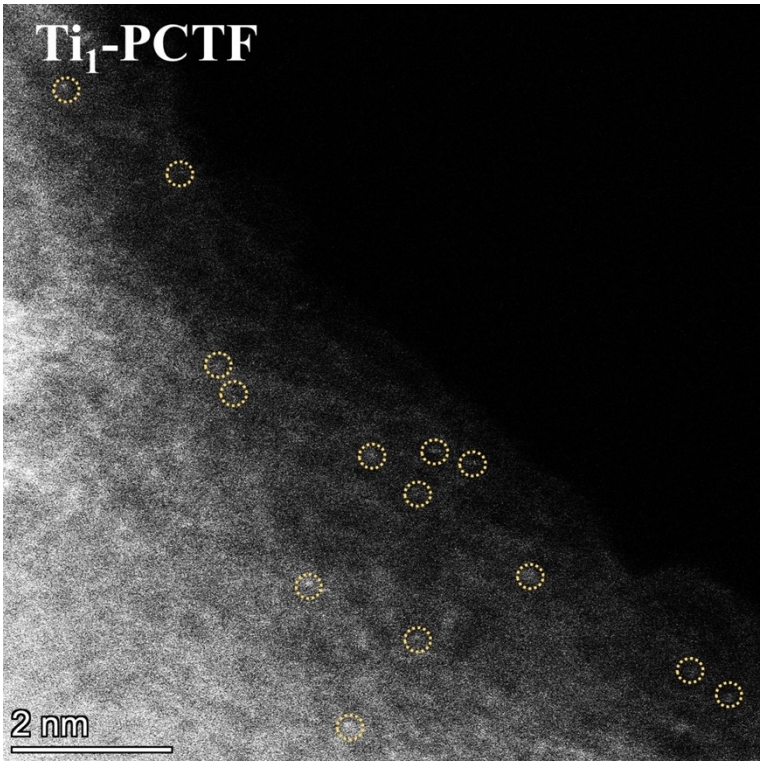

Fig. S23. The HAADF-STEM image of Ti_1-PCTF

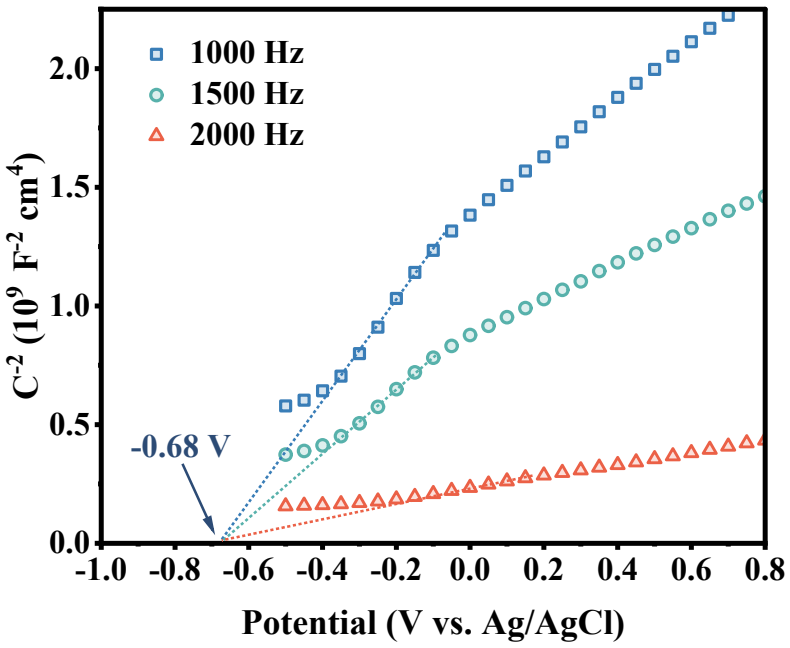

Fig. S24. Mott-Schottky plot of CTF at various test frequencies.

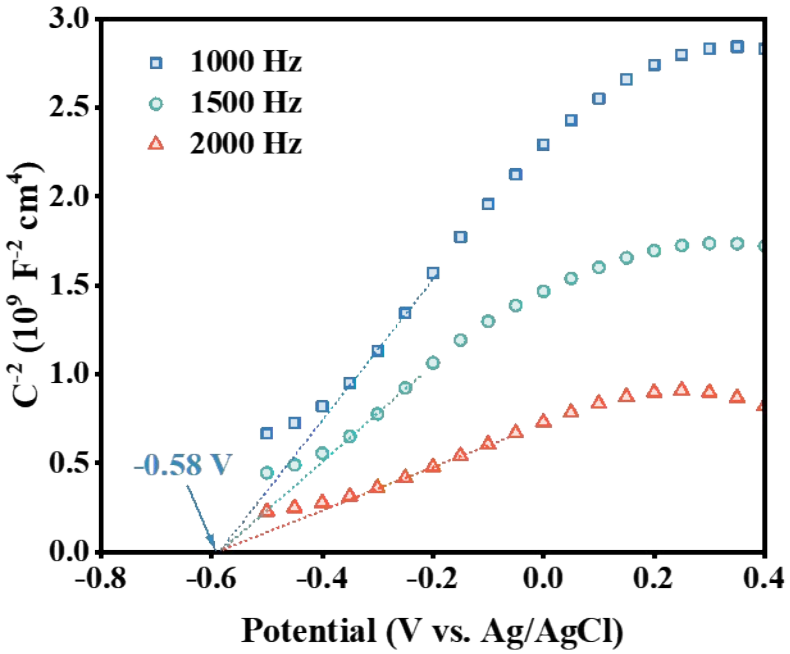

Fig. S25. Mott-Schottky plot of Co_1-CTF at various test frequencies.

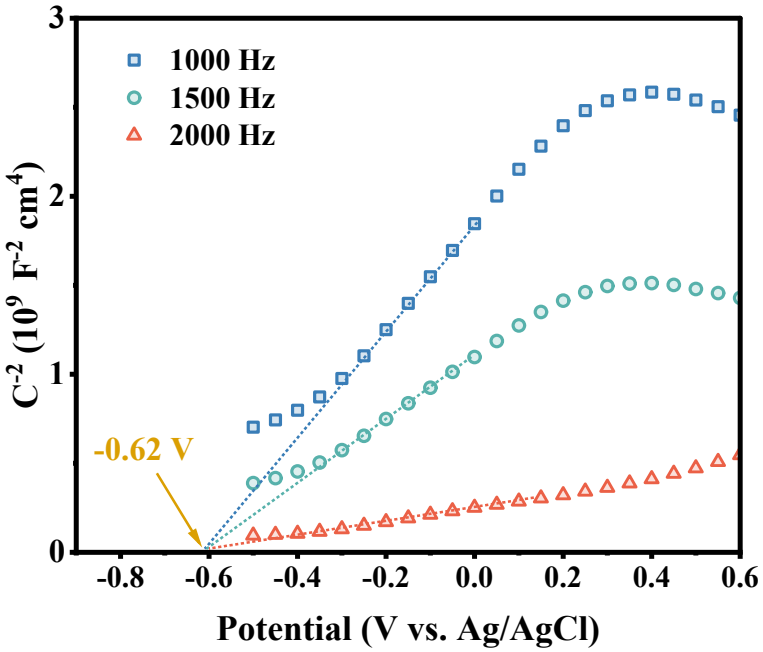

Fig. S26. Mott-Schottky plot of PCTF at various test frequencies.

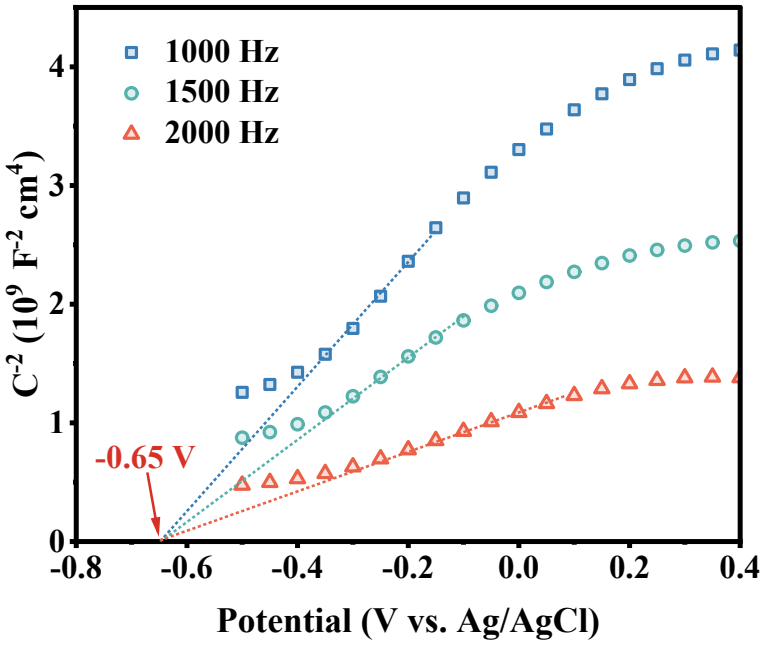

Fig. S27. Mott-Schottky plot of Co_1-PCTF at various test frequencies.

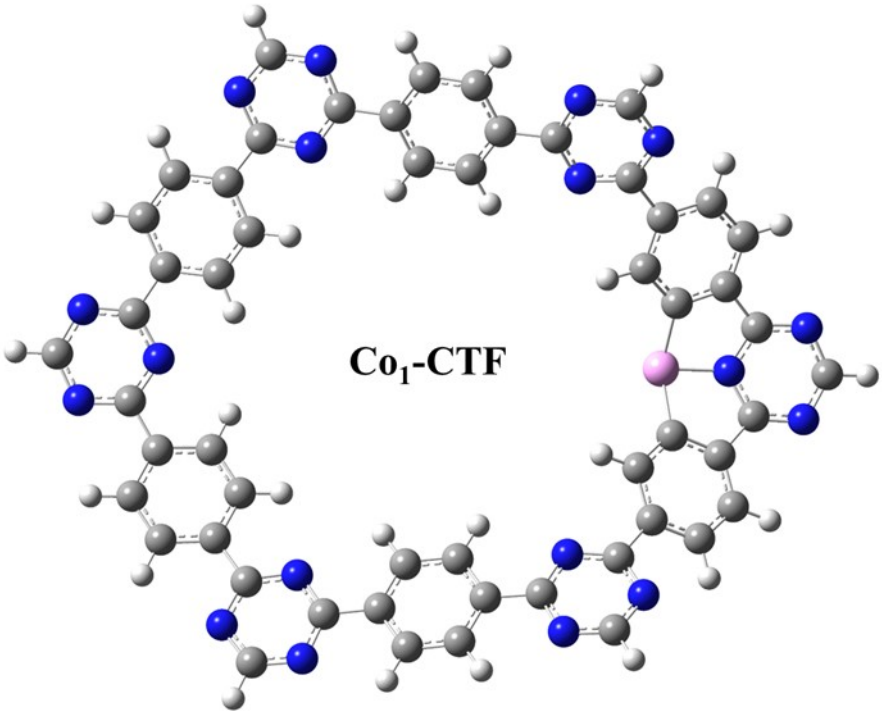

Fig. S28. The Co_1-CTF structure optimized by Gaussian computation.

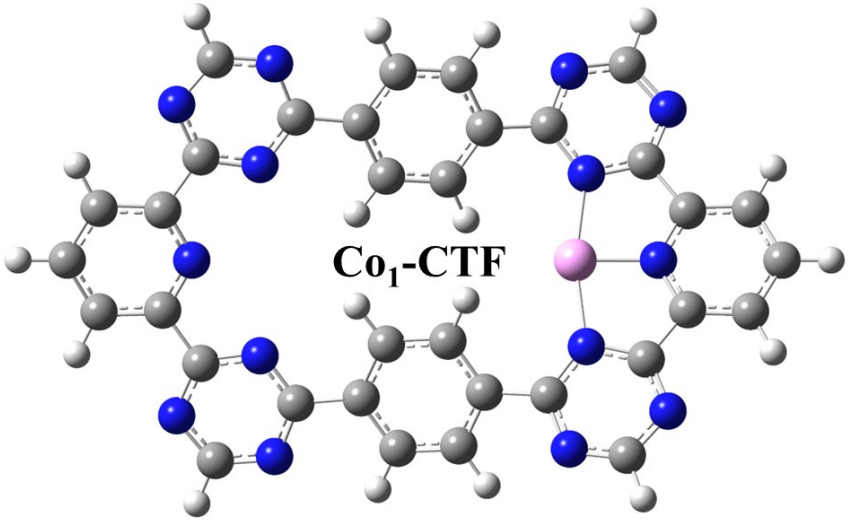

Fig. S29. The Co_1-PCTF structure optimized by Gaussian computation.

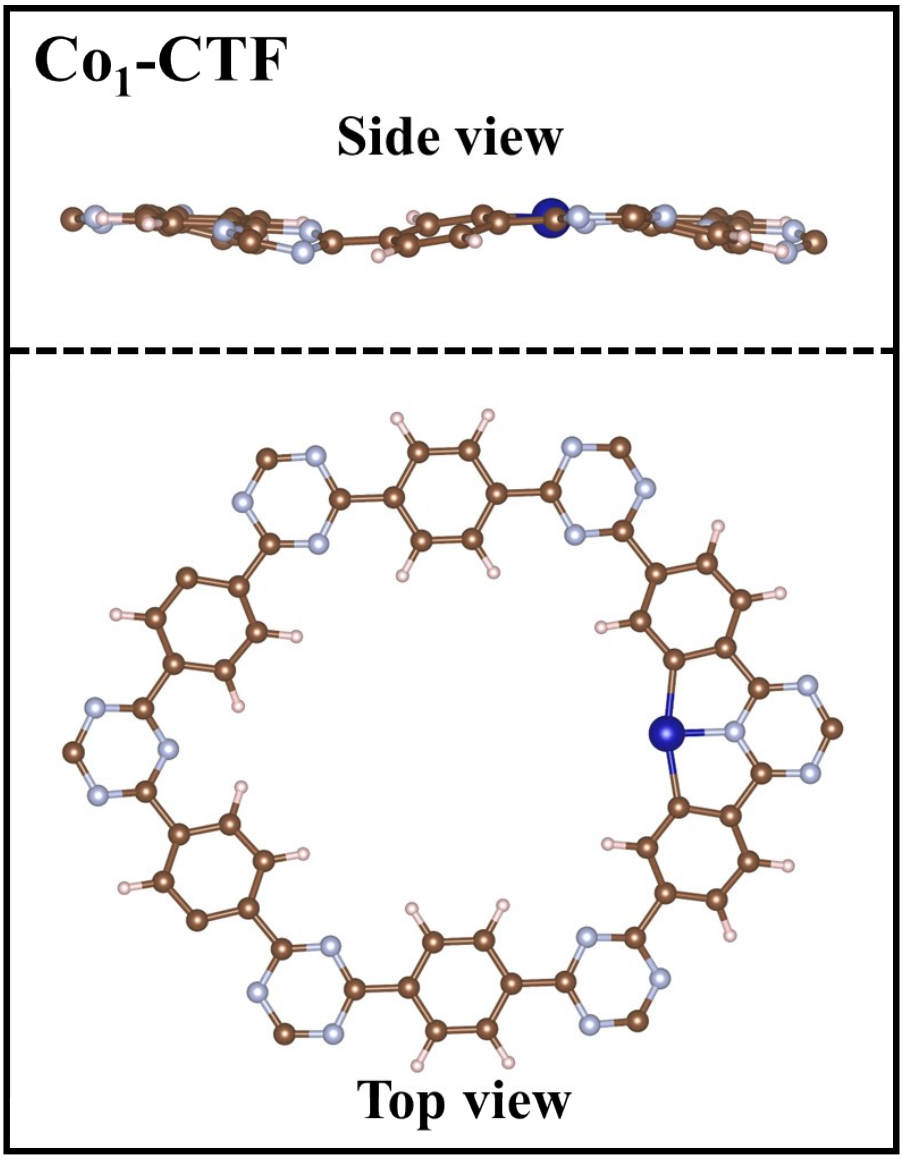

Fig. S30. Optimized geometry structures of Co_1-CTF at top and side view.

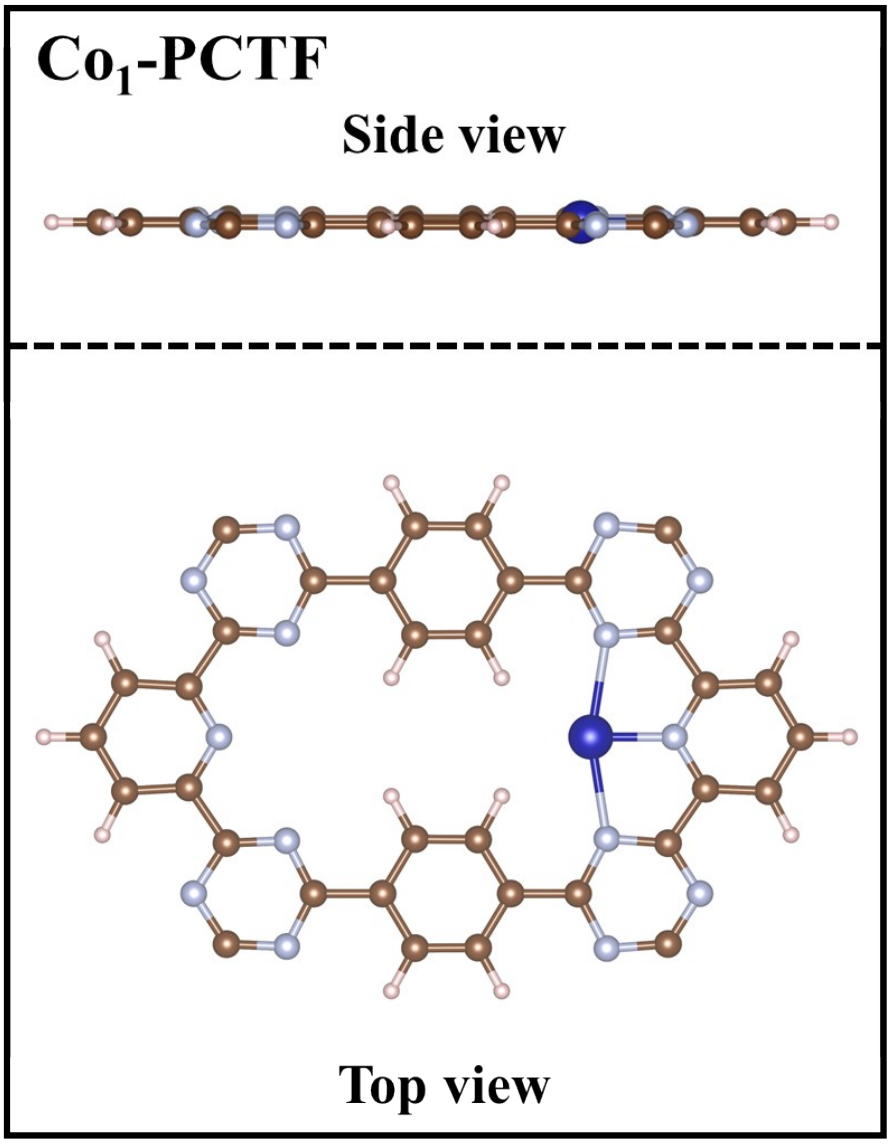

Fig. S31. Optimized geometry structures of Co_1-PCTF at top and side view.

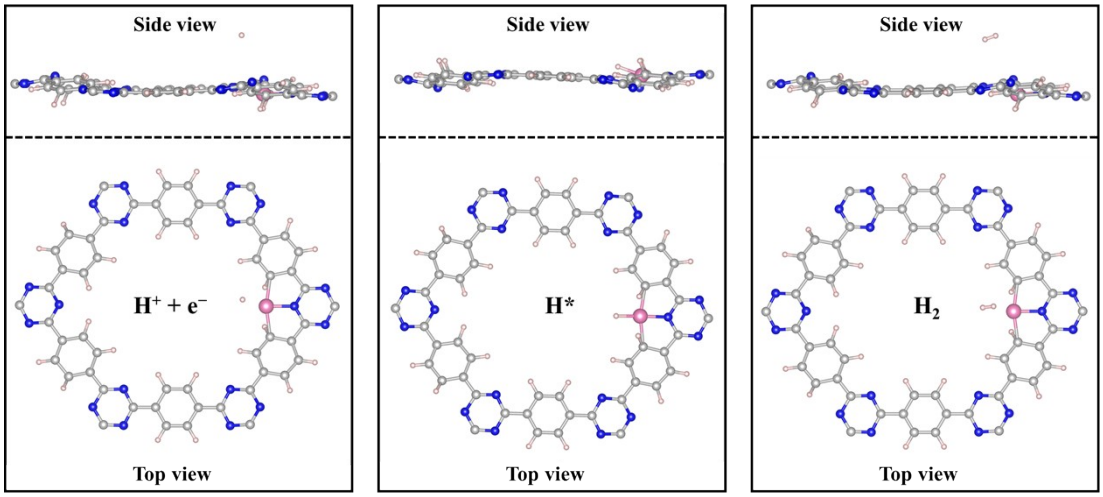

Fig. S32. Optimized structures of $H^+ + e^-$, H* intermediate and H_2 for Co_1-CTF.

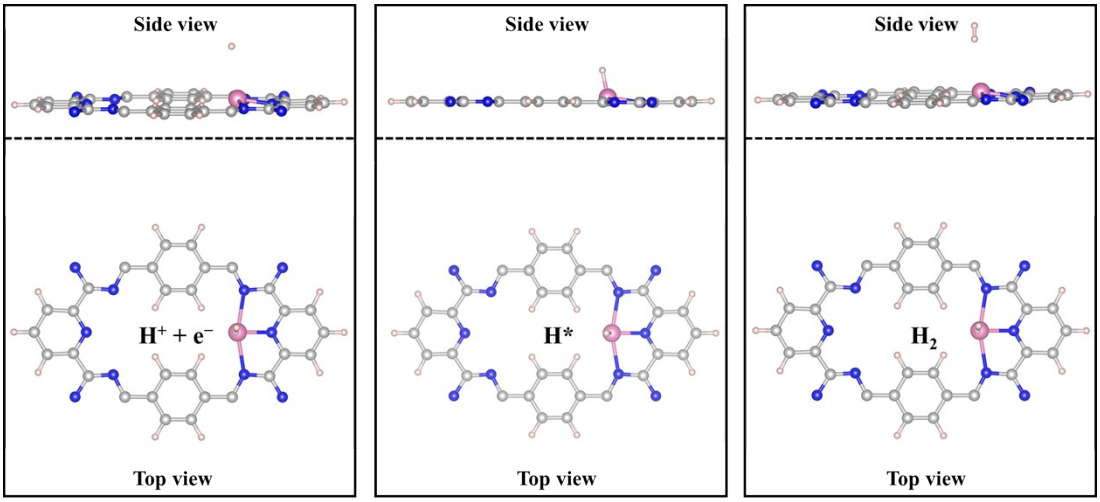

Fig. S33. Optimized structures of $H^+ + e^-$, H* intermediate and H_2 for Co_1-PCTF.

Table of Contents

Table S1. Quantitative EXAFS fitting results of Co-foil and Co_1-PCTF.

Samples	Absorption edge	Path	N[a]	R (Å)[b]	σ^2 (10^{-3}Å^2)[c]	ΔE_0 (eV)[d]	R-factor[e]
Co-foil	Co K-edge	Co-Co	12.0	2.47	3.53	3.23	0.0089
Co_1-PCTF	Co K-edge	Co-N	3.1	2.09	5.62	4.67	0.0151

[a] Coordination number; [b] R, distance between absorber and backscatter atoms; [c] σ^2, Debye-Waller factor to account for both thermal and structural disorders; [d] ΔE_0, inner potential correction; [e] R-factor indicates the goodness of the fit.

Table S2. Comparison of photocatalytic H_2 evolution rate of Co_1-PCTF with recently reported COF-based photocatalysts.

Catalyst	Photocatalytic H_2 evolution rate (μmol g^{-1} h^{-1})	Irradiation	dosage of catalyst (g L^{-1})	Reference
Co_1-PCTF	**2562.4**	**>420 nm**	**0.2**	**This work**
CTF-HUST-1	1460	>420 nm	0.5	[1]
CTF-HUST-2	2647	>420 nm	0.5	[1]
CTF-HUST-3	1238	>420 nm	0.5	[1]
CTF-HUST-4	1582	>420 nm	0.5	[1]
Sulfur-doped-CTF-1	2000	>420 nm	0.4	[2]
T3H-CTF	2028.06	>420 nm	0.83	[3]
$CTF\text{-}ES_{200}$	2000	>420 nm	0.3	[4]
CTF-amide-16	1133	>420 nm	0.4	[5]
CTF-HUST-C5	2400	>420 nm	0.5	[6]
CTF-HUST-C6	650	>420 nm	0.5	[6]
bulk-CTF	1619	>420 nm	0.2	[7]
CTF-Br-2	330	>420 nm	0.2	[8]
COF-ZIS	695	>420 nm	1	[9]
Py-N-DBT-COF	249	>420 nm	0.1	[10]
COF-TNOB-P2	1824	>400 nm	0.02	[11]
cobaloxime-modified COF	1900	>420 nm	0.2	[12]

Table S3. The AQY values for Co_1-PCTF.

Wavelength（nm）	Intensity（W·cm^{-2}）	Area（cm^2）	nH_2 (μmol)	N	AQY (%)
365	0.005105	10	28.650	3.37457E+20	10.222

400	0.003934	10	16.800	2.84986E+20	7.098
460	0.003923	10	9.753	3.26818E+20	3.593
490	0.002595	10	6.635	2.30284E+20	3.469
550	0.002124	10	5.987	2.11567E+20	3.407
580	0.001834	10	4.345	1.92645E+20	2.716

References

1 K. Wang, L. M. Yang, X. Wang, L. Guo, G. Cheng, C. Zhang, S. Jin, B. Tan and A. Cooper, *Angew. Chem. Int. Ed.*, 2017, **56**, 14149-14153.

2 L. Li, W. Fang, P. Zhang, J. Bi, Y. He, J. Wang and W. Su, *Journal of Materials Chemistry A*, 2016, **4**, 12402-12406.

3 X. Han, F. Zhao, Q. Shang, J. Zhao, X. Zhong and J. Zhang, *ChemSusChem*, 2022, **15**, e202200828.

4 Z. A. Lan, M. Wu, Z. Fang, Y. Zhang, X. Chen, G. Zhang and X. Wang, *Angew. Chem. Int. Ed.*, 2022, **61**, e202201482.

5 Z. Li, T. Li, J. Miao, C. Zhao, Y. Jing, F. Han, K. Zhang and X. Yang, *Science China Materials*, 2023, **66**, 2290-2298.

6 M. Liu, Q. Huang, S. Wang, Z. Li, B. Li, S. Jin and B. Tan, *Angew. Chem. Int. Ed.*, 2018, **57**, 11968-11972.

7 T. Sun, Y. Liang and Y. Xu, *Angew. Chem. Int. Ed.*, 2022, **61**, e202113926.

8 L. Guan, G. Cheng, B. Tan and S. Jin, *Chemical Communications*, 2021, **57**, 5147-5150.

9 C. Cui, X. Xu, X. Zhao, N. Xi, M. Li, X. Wang, Y. Sang, X. Yu, H. Liu and J. Wang, *Nano Energy*, 2024, **126**, 109632.

10 X. Ren, J. Sun, Y. Li and F. Bai, *Nano Research*, 2024, **17**, 4994-5001.

11 G. Fu, R. Ma, S. Xu, T. Xu, S. Li, Y. Zhao, Y. Jing, X.-B. Li and T. Zhang, *Materials Today Energy*, 2024, **40**, 101477.

12 S. Wang, T. Wu, S. Wu, J. Guo, T. He, Y. Wu, W. Yuan, Z. Zhang, Y. Hua and Y. Zhao, *Angew. Chem. Int. Ed.*, 2023, **62**, e202311082.